iScience

CellPress

Article

A Moisture-Penetrating Humidity Pump Directly Powered by One-Sun Illumination

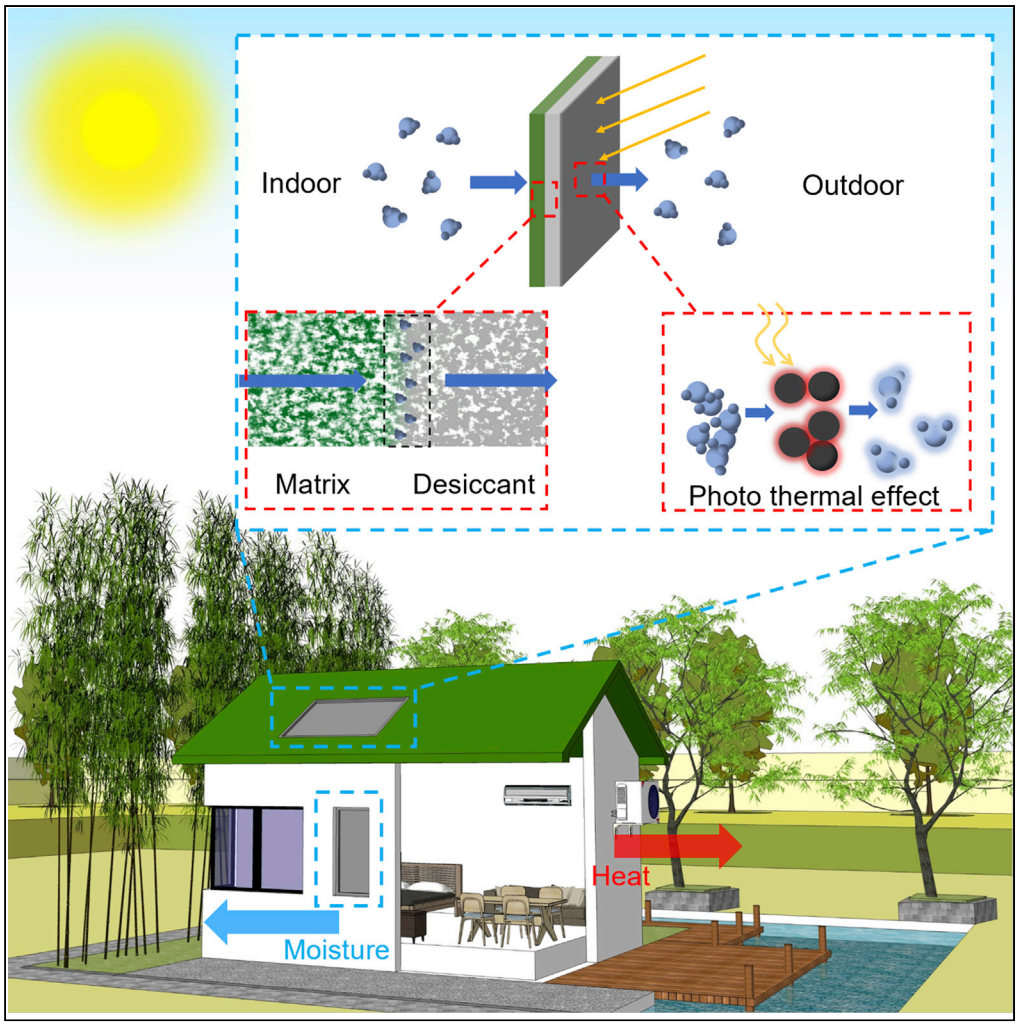

Biye Cao,
Yaodong Tu,
Ruzhu Wang

rzwang@sjtu.edu.cn

HIGHLIGHTS

We propose a concept of moisture-permeable panel that enables moisture penetration

A humidity pump prototype using the moisture-permeable panel is designed

The humidity pump can reduce the indoor relative humidity to a medium level

Cao et al., iScience *15*, 502–513
May 31, 2019
https://doi.org/10.1016/j.isci.2019.05.013

iScience

CellPress

Article

A Moisture-Penetrating Humidity Pump Directly Powered by One-Sun Illumination

Biye Cao,[1] Yaodong Tu,[1] and Ruzhu Wang[1,2,*]

SUMMARY

There is broad demand for humidity control for industrial, commercial, and residential applications. Current humidity pumping technologies require intensive maintenance because of the complexity of their mechanical structures. Furthermore, indirect utilization of solar energy increases both cost and energy loss. Here, we demonstrate a new humidity pumping concept based on multilayer moisture permeable panels. Such panels, with a simple structure, may allow the penetration of moisture from indoor (adsorption) to outdoor (desorption) with little heat loss. One-sun illumination is introduced as the direct energy source. A proof-of-concept prototype is designed and established, successfully dehumidifying indoor air with the best dehumidification rate of 33.8 $g \cdot m^{-2} \cdot h^{-1}$. By applying such humidity pump, the indoor latent heat load can be handled independently, without any auxiliary unit, thus consuming no electricity.

INTRODUCTION

Ambient humidity collection has become a popular topic because of its important role in water collection and air humidity adjustment, according to the different post-collection management processes. Atmospheric water harvesting, which aims to obtain clean liquid water after ambient humidity collection, has already been intensively studied (Kim et al., 2017; Mekonnen and Hoekstra, 2016; Kalmutzki et al., 2018). This contributes significantly to arid areas with potable water shortage. Humidity control, which focuses on the removal of water vapor in the air after humidity collection, also attracts dramatic attentions owing to the increasing interest on sustainable buildings (Allouhi et al., 2015; Anand et al., 2015; Grossman, 2002; Otanicar et al., 2012). In modern times, nearly 40% of the total energy consumption is associated with buildings worldwide (Zhao and Magoules, 2012; Farese, 2012; Yang et al., 2014; Costa et al., 2013). According to the United Nations, by 2050, 70% of the total population or more is trending to live in urban areas, where the density of buildings is significantly larger than countryside and people usually spend more than 80% of days indoors (Rupp et al., 2015). This makes the indoor environment control dramatically important (Yang et al., 2014), and thus increasing attention has been paid to this field. Evidence shows that more than half of energy consumption in buildings, which is equal to almost 20% of the total energy consumption, results from air-conditioning systems (Farese, 2012; Costa et al., 2013; Yang et al., 2014). Besides, temperature and humidity management is also critical in many industrial occasions (Nkwetta and Sandercock, 2016). As widely acknowledged, roughly 40% of the heating, ventilation, and air-conditioning (HVAC) load is responsible for latent heat load (dehumidification) and the other 60% for sensible heat load (Tu et al., 2017). Thus effective technologies for humidity control would be of great importance. Conventional vapor compression system, which is the most preferred dehumidification technology commercially, dehumidifies the air through the dew point method, by which the supply air is cooled down to a much lower temperature than the indoor environment needs, whereas the moisture in the air is condensed and removed (Zhang et al., 2014). However, a reheating of outlet air is essential to satisfy the temperature needs of inhabitants and thus results in large extra energy consumption. Previous researches have shown that the temperature- and humidity-independent control system, in which the sensible and latent heat loads are regulated separately, has a promising energy-saving potential (Zhang et al., 2014; Zhao et al., 2011; Zhang and Liu, 2016). Therefore different dehumidification technologies based on ambient humidity collection process have been developed to achieve the expected balance between energy consumption and indoor thermal comfort. The solid desiccant cooling system may handle the latent heat load independently and use waste heat or renewable energy, such as solar energy. The refrigerant and desiccant materials involved are mostly environment friendly. This may result in obvious energy-saving potential and positive ecological and economic effects (Daou et al., 2006; Panaras et al., 2011; Zheng et al., 2014; La et al., 2010). The rotary system, based on solid desiccant system, can handle the latent heat load continuously and more efficiently (La et al., 2010). The liquid desiccant absorption system, which

[1]Institute of Refrigeration and Cryogenics, Department of Mechanical Engineering, Shanghai Jiao Tong University, 800 Dongchuan Road, Shanghai 200240, P.R.China

[2]Lead Contact

*Correspondence: rzwang@sjtu.edu.cn

https://doi.org/10.1016/j.isci.2019.05.013

utilizes the hygroscopic salt solution instead of a solid desiccant, can adjust the indoor humidity accurately and continuously (Mei and Dai, 2008; Shukla and Modi, 2017). In recent years, the desiccant-coated heat exchanger system is developing very fast, with merits of both vapor compression system and sorption-based system (Tu et al., 2017; Zheng et al., 2015a, 2015b). The solid desiccant material is coated on the fins of the heat exchanger so that the latent and sensible heat loads can be handled independently and simultaneously. As the concept of sustainable building or zero energy building is receiving increasing impetus, several novel ideas on energy-saving technologies in buildings flourished regarding different aspects (Rotzetter et al., 2012; Marszal et al., 2011; Deng et al., 2014). Renewable energy resources, in most cases the solar energy, are usually the first choice (Chu and Majumdar, 2012). Thus the sorption-based dehumidification technologies become very promising choices for indoor air-conditioning in buildings.

However, the sorption-based dehumidification technologies are still not that widely applied currently. Some major drawbacks still limit the application in industries and buildings. Owing to the adsorption-desorption nature, the working process is usually intermittent (Panaras et al., 2011; La et al., 2010). The installation, especially the rotary system, although overcomes the intermittence problem, is often bulky and complex, and this inevitably increases the maintenance cost a lot (La et al., 2010). Furthermore, such systems can only utilize solar thermal energy by introducing additional energy harvesting, conversion, and transportation units and systems, which is also a major reason for bulky and complex installation (Daou et al., 2006). The direct usage of solar energy is attracting attention currently, and a large amount of research has been carried out regarding the high-efficiency usage of solar thermal energy in surface-localized heating and vapor generation (Ni et al., 2016; Wang et al., 2014; Liu et al., 2015a, 2015b). However, unfortunately few such researches have been related with the sorption-based humidity control technologies, which should have a large potential.

In this study, a moisture-permeable panel based on solid desiccant directly powered by one-sun illumination is proposed to serve as a passive humidity pump, which can transfer the moisture in the air from indoor to outdoor with a very simple structure. We also report a proof-of-concept prototype that successfully removes the indoor moisture to outdoor using our passive humidity pump only under one-sun illumination. We introduced both silica gel (SG)-based and SG-MIL101(Cr)-based moisture permeable panels for comparison. The MIL-101(Cr) can improve the dehumidification rate and also successfully reduce the relative humidity (RH) down to the medium level (around 50%), which fulfills the human thermal comfort requirement (Wan et al., 2009). With such technologies, the indoor latent heat load can be handled independently without consuming electricity and the HVAC systems in buildings are expected to be much more efficient.

RESULTS

The Concept and Design of the Moisture-Permeable Panel

The moisture-permeable panel consists of three parts: the porous substrate, the desiccant layer, and the photothermal coating film (see Figure 1A). The porous substrate is introduced for both holding the desiccants and providing good thermal insulation property. The widely used desiccants, such as vermiculite or zeolite powders, are inconvenient and difficult to be shape stable, thus a matrix that may provide skeletons for desiccants to attach is essential. Besides, to prevent the heat loss of the panel, thermal insulation property should be considered. The desiccant layer is responsible for adsorbing water vapor from indoor space, transferring the water molecules from the inner to the outer surface and desorbing the attached water to outdoor space. To achieve such function, a relatively good water capture ability is expected under normal room temperature and humidity, and its desorption should happen under relatively modest temperature. The photothermal layer is introduced to provide sufficient desorption heat. Different from the traditional desorption process, the heat is neither coming from hot air, which flows over the desiccant layer surface, nor from the heat exchanger fins, which are coated by desiccant, both of which are energy-consuming processes. Instead, the needed heat is directly generated on the desiccant layer surface, which largely simplifies the installation of the structure. The photothermal layer should be made from a material that is very inert and stable considering the variable and even extreme outdoor environment.

In this research, a common thermal insulation foam, the wet foaming phenolic foam (PF), is introduced as the porous substrate due to its merits of excellent thermal insulation, low cost, easy shaping, etc. Glass and ceramic fibers are also promising alternatives, which are more rigid but suffer from greater weight and difficult shaping issues. For the desiccant layer, the SG and SG-MIL101(Cr) composite materials are chosen and investigated. Silica gel is widely applied in adsorption cooling and dehumidification fields owing to its

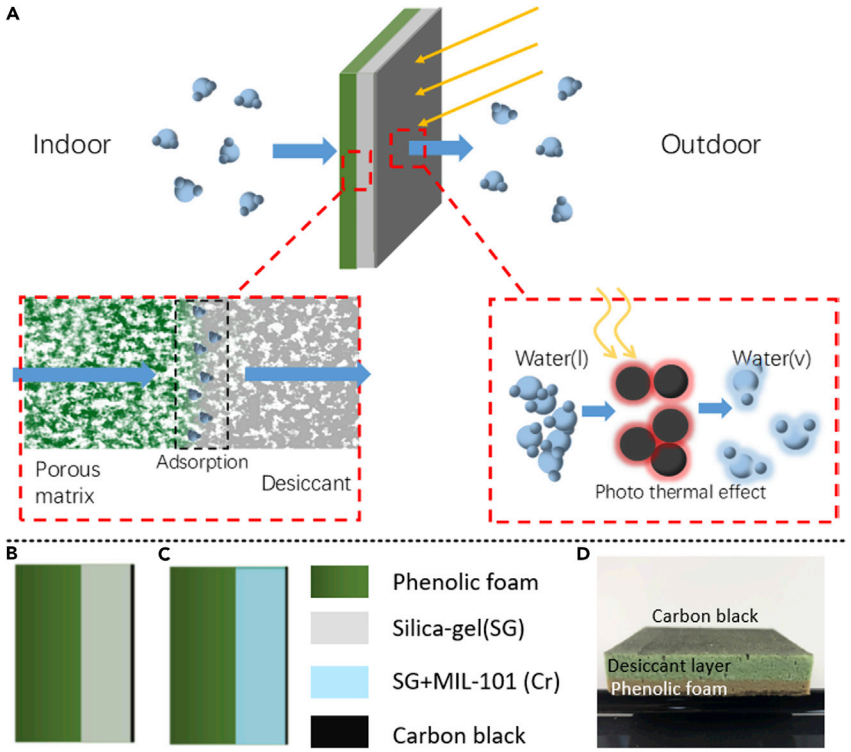

Figure 1. An Overview of the Moisture Permeable Panel

(A–D) (A) Schematic structures of moisture-permeable panel and expected moisture transfer path. The moisture in the indoor air passes through the porous matrix and is adsorbed by desiccant. The absorbed water molecules pass through the desiccant layer and reach the outdoor surface. The absorbed water is removed by the heat generated by CB powder under sunlight illumination. The panel structure with different desiccant layers is shown. (B) SG layer and (C) MIL101(Cr)-SG layer. (D) Photograph of the cross section of a real moisture-permeable panel.

advantages of satisfying water capture ability, non-toxic nature, easy fabrication process, and low cost (Pesaran and Mills, 1987a, 1987b). It plays an important role especially in rotary wheel systems and desiccant-coated heat exchanger systems (Tu et al., 2017; Ge et al., 2009; Zheng et al., 2015a). The metal organic framework MIL-101(Cr) has been investigated and applied in several cases such as carbon dioxide capture, hydrogen storage, or water adsorption (Rallapalli et al., 2013; Liu et al., 2013; Hong et al., 2009; Khutia et al., 2013). Here it is chosen as the second candidate because it also enjoys excellent water adsorption ability and stability under extreme weather conditions (hot and strong sunshine) (Ferey, 2005). Besides, it has a type V isotherm according to International Union of Pure and Applied Chemistry, and the S-shape is around medium level (see Figure S1), which is the optimum feature for solid desiccant system. The photothermal layer is made from carbon black (CB) powder with particle size around 50 nm. This very small size may guarantee good dispersion of CB powder on the panel surface. By following the ideas above, two kinds of panels, one with pure SG layer and the other with SG-MIL101(Cr) layer, have been proposed and fabricated, as shown in Figures 1B and 1C (see Figure S4, Transparent Methods section for details of MIL-101Cr fabrication and moisture-permeable panel fabrication). A cross-sectional photograph of a real panel sample is shown in Figure 1D for better understanding. The detailed fabrication process is shown in Transparent Methods. It should also be noted that two structures of desiccant layer are applied, either condensed or loose, according to the amount of desiccant in the layer. Details for each panel are listed in Table S1.

Different Desiccant Layer Structures with Different Mass Transfer Abilities

The scanning electron microscopic and transmission electron microscopic (TEM) images of panels are first given to understand the panel surface morphology (Figure 2). Figure 2A clearly shows the pure PF surface structure. The pores around the skeletons are more than 100 μm, which provides enough space for both desiccant adhesion and moisture transport. In the condensed layer (Figure 2B), most of the pores are filled with SG, and this is expected to result in a larger adsorption quantity. On the contrary, the loose layer

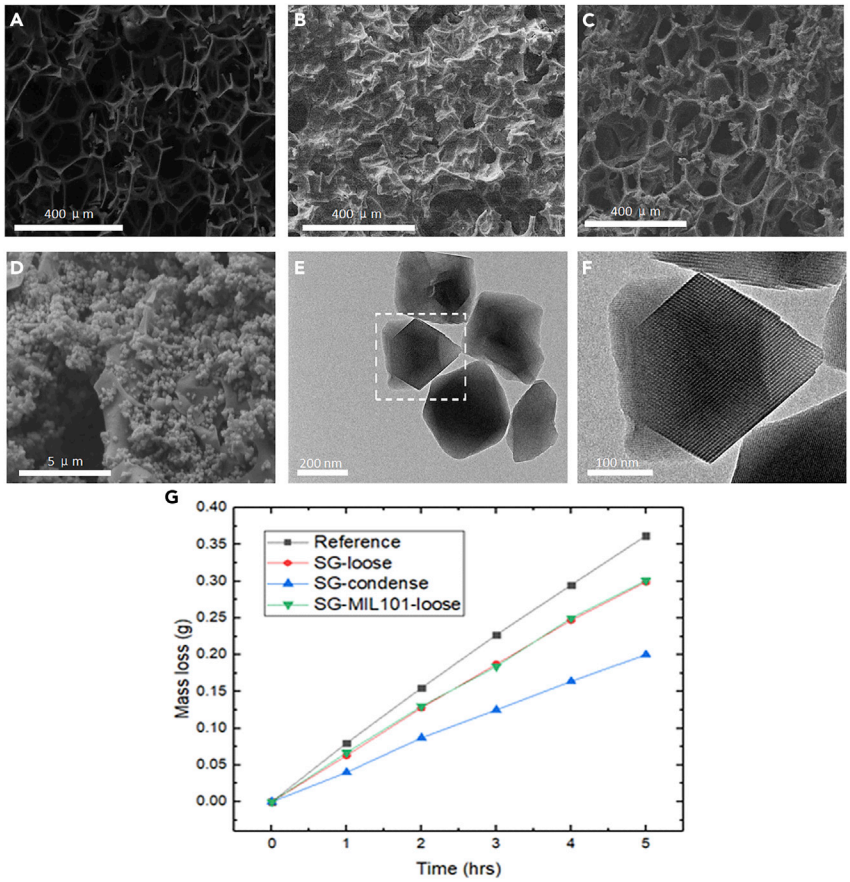

Figure 2. Surface Morphologies and Water Vapor Transmission Test

Scanning electron microscopic images of (A) pure wet-foaming phenolic foam surface, (B) PF foam with condensed SG layer, (C) PF foam with loose SG layer, and (D) MIL-101(Cr) aggregates on the SG particle surface. TEM images of (E) pure MIL-101(Cr) crystals and (F) the zoomed-in area of dashed square in (E). (G) Results of permeability test. The reference sample in permeability test stands for the pure wet-foaming phenolic foam without any silica gel attachment.

(Figure 2C) spares more pores so that more channels can be involved in mass transfer instead of being blocked. However, the influence of less adsorption amount should be further evaluated. Figure 2D gives the details of SG-MIL101(Cr) composite desiccant. Very small MIL101(Cr) crystals are observed to be aggregated on the SG surface (and also inside the SG bulk). The TEM images provide clear appearance of the MIL101(Cr) crystals (Figures 2E and 2F). The dimension of single MIL101(Cr) crystal is around a few hundred nanometers, and very regular pore and channel structures can be seen in Figure 2F. The dynamic water adsorption and also nitrogen adsorption of the MIL101(Cr) involved are shown in Figure S2.

To acquire detailed evidence on mass transfer, the water vapor transmission (WVT) test was carried out (see Figure S5, Transparent Methods, Water Vapor Transmission Test for experimental details). The mass loss of each kind of panel was weighed and is shown in Figure 2G, in which the slope of the line indicates the mass decrease rate proportion to WVT ability. The reference (black square) curve represents the pure PF foam sample, whereas red dots, blue triangles, and green triangles stand for panels with loose SG, condensed SG, and loose SG-MIL101(Cr) composite layers, respectively. All the mass loss curves show a linear shape. It is obvious that the impregnation of SG into the PF foam diminishes the moisture transmission ability, and the more SG there exists, the worse the mass transfer rate is. The addition of MIL-101(Cr) hardly influences the WVT ability, and the two lines of SG loose layer and SG-MIL-101(Cr) layer are mostly identical. This is attributed to the tiny particle size and very small aggregation domains of MIL-101(Cr). As presented in Figure 2D, the aggregated domains are in the range of less than 1 μm and the particles are even much smaller, which can be considered as a thin film covering the SG surface. These MIL-101Cr particles and aggregated domains barely change the pore and channel structures and thus consequently influence very little on the

Desiccant Layer Structures	Mass Loss Rate ($g \cdot h^{-1}$)	WVT ($g \cdot h^{-1} \cdot m^{-2}$)	Permeance ($g \cdot h^{-1} \cdot m^{-2} \cdot pa^{-1}$)	Permeability ($g \cdot h^{-1} \cdot m^{-1} \cdot pa^{-1}$)
SG condensed	0.0400	44.4	0.0226	$1.13x10^{-4}$
SG loose	0.0598	66.4	0.0338	$1.69x10^{-4}$
SG-MIL-101(Cr)	0.0584	64.8	0.0330	$1.65x10^{-4}$

Table 1. The Mass Loss Rate, WVT, Permeance and Permeability of Moisture-Permeable Panels with Different Desiccant Layer Structures

WVT ability. This result corresponds to our suggestion above that the amount of accessible channels and pores in the desiccant layer are considered as the dominating reasons.

Quantitatively, the specific indicators, WVT, water permeance, and permeability, can be expressed by the following equations according to the Standard Test Methods for Water Vapor Transmission of Materials:

$$WVT = \frac{G}{tA} \quad \text{(Equation 1)}$$

where G stands for the total mass decrease amount (in g), t is the time (h), and A is the area of the sample mouth (in m^2).

$$\text{permeance} = \frac{WVT}{\Delta p} = \frac{WVT}{S(R_1 - R_2)} \quad \text{(Equation 2)}$$

where Δp indicates the vapor pressure difference between two sides of the tested samples, S is the saturation vapor pressure under test temperature, and R_1 and R_2 are the RHs between two sides of the tested samples.

$$\text{average permeability} = \text{permeance} \times \text{thickness} \quad \text{(Equation 3)}$$

The sample mouth area is 9 cm^2 (3cmx3cm), and the test environment is carefully controlled at 23°C and 50% RH. Thicknesses of all the samples are identical. Using the equations introduced above, the WVT and water permeance of each sample are calculated. The detailed results are listed in Table 1. Basically, the WVT and permeance of panels with loose SG layer are 1.5 times higher than those of panels with condensed SG layer and are almost identical to those of panels with SG-MIL101(Cr) composite desiccant layer. So it is very obvious that both loose SG and loose SG-MIL101(Cr) composite layers have good mass transfer abilities, whereas that of the condensed layer is much worse (see also Figure S3, Table S3, and Transparent Methods, The Sorption Rate Test for more information on sorption dynamics).

The Surface Temperature (Regeneration Temperature) Enhancement by the Carbon Black Photothermal Layer

Infrared (IR) images were taken to evaluate the photothermal effect induced by the CB coating, as shown in Figure 3. Four samples with different structures and initial conditions were placed under the same light source with 1,000 W/m^2 intensity. The details of each sample are listed in Table 2. Photographs were taken after 0, 5, and 30 min, and all the samples (except sample D) reached equilibrium at 25°C, 70% RH working condition before they are exposed to illumination. A relatively small temperature rise of sample A (average temperature: 37.7°C after 5 min) is observed, whereas sample B has a much faster temperature increase (average temperature: 56.7°C after 5 min). This can be ascribed to the CB coating on the surface, which generates much more heat due to the photothermal effect. Sample D, which has identical structure to sample B, is pre-dried completely before taking photograph and thus resulted in an even higher surface temperature (average temperature: 58.4°C after 5 min) because water desorption usually consumes a certain amount of heat. Sample C, which has an SG-MIL101(Cr) composite desiccant layer, has a lower temperature distribution (average temperature: 47.0°C after 5 min). The dominating reason is believed to be the larger water capacity of the composite desiccant and faster water-losing rate. More detailed information can be seen in Table S2. The IR images clearly prove that the CB coating can largely increase the surface temperature. Besides, the desorption can happen under one-sun illumination condition according to the lower temperature of samples B and C, and obviously the composite desiccant desorbs water faster than the pure SG (also see Figure S2). A heat transfer model that applies the CB layer as a surface heat source is established, and the simulation also shows the same trend as Figures 2B and 2D (see Transparent Methods, Model and Simulation, and Figures S6 and S7).

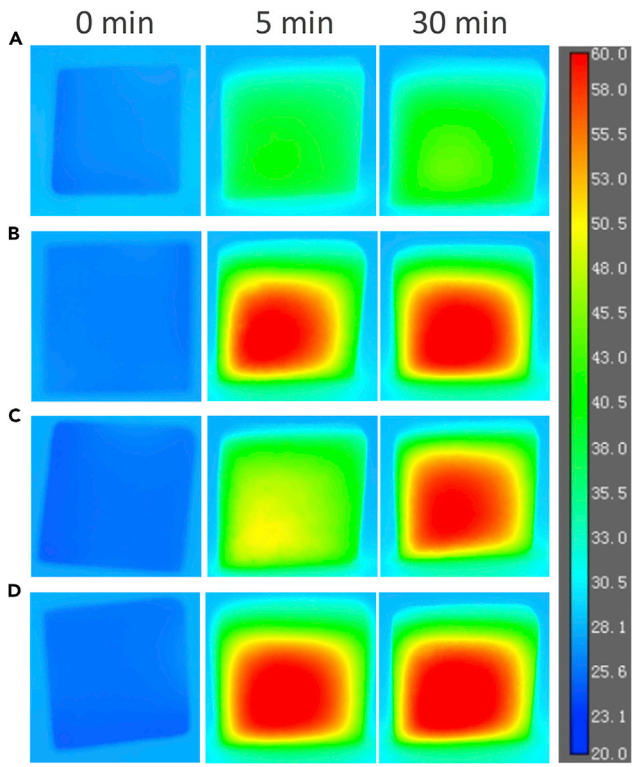

Figure 3. IR Images of Different Panels under One-Sun Illumination after a Fixed Time

(A–D) (A) Wet panel with SG layer, surface without CB coating; (B) wet panel with SG layer, surface with CB coating; (C) wet panel with MIL101-SG layer, surface with CB coating; (D) dry panel with SG layer, surface with CB coating.

Proof-of-Concept Prototype and Dehumidification Results

To demonstrate the feasibility and to evaluate the performance of this novel moisture pump under real working conditions, a proof-of-concept prototype applying the moisture permeable panel was established and tested. A scaled down model of a house was made with dimensions of 70 cm × 40 cm × 40 cm. Figure 4A gives the sketch of this prototype. Two windows with an area of 5 cm × 5 cm were design for MP panel installation. Movable outer shields and inner shields were introduced for shielding the sunlight or the indoor air depending on different working processes. By opening the inner shield of one MP panel, this panel absorbs water vapor from the indoor air, whereas the outer shield is closed, keeping this panel from sunlight illumination. Meanwhile, the inner shield of the other panel is closed, whereas the outer shield is opened, isolating this second panel from indoor air but under illumination from sunlight, as shown in Figure 4B. After a certain period, the shields are switched and the panel working condition is reversed. The first panel, which has absorbed a certain quantity of water, is now exposed to sunlight, whereas the other panel, which has been regenerated well, is now capturing the water vapor from indoor space, as shown in Figure 4C. By switching the working mode alternatively in a controlled period, this system absorbs indoor water vapor and loses water to outdoor simultaneously.

Two identical MP panels with 5 cm × 5 cm area were installed in each window. The initial working condition inside the box was 25°C, 65% RH, and both panels reach equilibrium under such working condition. The box was tightly sealed to prevent any possible leakage, and one panel with inner shield closed was exposed to one-sun illumination (1,000 $W \cdot m^{-2}$), whereas the other panel was still covered by outer shield. The switch time period was chosen as 20 min. After the switch, the working mode of each panel was changed, and this switch repeated within the whole dehumidification process. The outside working condition was kept constant at 25°C, 70% throughout the whole experiment. Figure 4D presents the results of this prototype applying panels with both SG loose layer (open cycles) and SG-MIL-101(Cr) layer (closed cycles), and several consecutive cycles of each panel were chosen and presented. For SG loose layer panel, obvious drop of RH (open cycle, blue) as well as water content (open cycle, black) appeared in the early periods,

Sample	a	b	c	d
Desiccant	SG	SG	SG-MIL101(Cr)	SG
CB coating	No	Yes	Yes	Yes
Dry or wet	Wet	Wet	Wet	Dry

Table 2. Details of Each Sample in IR Images

indicating the adsorption of water vapor by the desiccant layer in the panel and the decrease of RH of the indoor space. However, as the setup kept working and the RH went down (around 60%), the RH drop became more and more subtle and finally reached a near-constant status. The indoor temperature remained almost constant, and only very small temperature variation was observed (less than 0.3°C) resulting from adsorption heat. This is associated with the thermal insulation layer because most of the adsorption heat generated in the desiccant layer spreads through the desiccant layer rather than the porous thermal insulation layer, leaving the inside temperature almost unchanged. The specific dehumidification rate can be calculated as follows:

$$r = \frac{\Delta m}{t \cdot S}\left(g \cdot m^{-2} \cdot h^{-1}\right) \quad \text{(Equation 4)}$$

where Δm (g) stands for the water loss during the whole dehumidification process, t represents the time (h), and S stands for the total area of the MP panels (m^2)

$$m = d \cdot m_{air} = d \cdot V \cdot \rho\ (g) \quad \text{(Equation 5)}$$

$$d = 0.622\frac{RH \cdot P_S}{B - RH \cdot P_S}\left(g \cdot kg^{-1}\right) \quad \text{(Equation 6)}$$

where d is the water content (g/kg) of the air, V is the volume of the model house, ρ is the density of air at the working temperature, RH is the relative humidity (%), P_s is the saturated water vapor pressure at the working temperature, and B stands for the atmospheric pressure.

For the panel with SG layer, only the first three cycles were taken into consideration. The indoor RH dropped from 65.0% to 62.2%, and the water content correspondingly varied from 12.74 to 12.29 $g \cdot kg^{-1}$, resulting in an average dehumidification rate of r = 24.2 $g \cdot m^{-2} \cdot h^{-1}$.

For the panel with SG-MIL101(Cr) layer (closed cycles), the performance was much better. During the first three cycles, the RH dropped obviously faster than that of the SG layer panel did. When the RH (closed cycles, blue) reached around 60%, the drop rate decreased to a moderate level but still kept going down regardless of this medium RH condition. The following several cycles clearly showed that the RH kept going down to a much lower value. Furthermore, Figure 4E presents a few cycles of SG-MIL101Cr panel working under much lower RH condition (around 52%, the medium RH level). Under such working condition, the indoor RH can still be steadily decreased. This is the major difference between SG-MIL101Cr layer and the SG layer. It is evident that the SG lost most of the dehumidification ability under such indoor-outdoor working conditions. However, the MIL101Cr can still have satisfactory water adsorption ability under the same condition, as described above in The Concept and Design of the Moisture-Permeable Panel. Below 60% RH, what contributes to the RH drop is only the MIL101Cr rather than SG.

To evaluate the dehumidification rate quantitatively, the process should be divided into two regions: the high-RH region (higher than 60%) and the medium-RH region (lower than 60%). At the high-RH region, the water content dropped from 12.76 to 12.13 $g \cdot kg^{-1}$ with an average dehumidification rate of r = 33.8 $g \cdot m^{-2} \cdot h^{-1}$. At the medium-RH region, the water content decreased from 12.13 to 11.59 $g \cdot kg^{-1}$ with an average dehumidification rate of r = 15.1 $g \cdot m^{-2} \cdot h^{-1}$. A brief model is established to theoretically estimate the dehumidification rate (see Transparent Methods, Dehumidification Rate).

The energy efficiency is calculated as follows:

$$\eta = \frac{H_{de}}{Q_{input}} \quad \text{(Equation 7)}$$

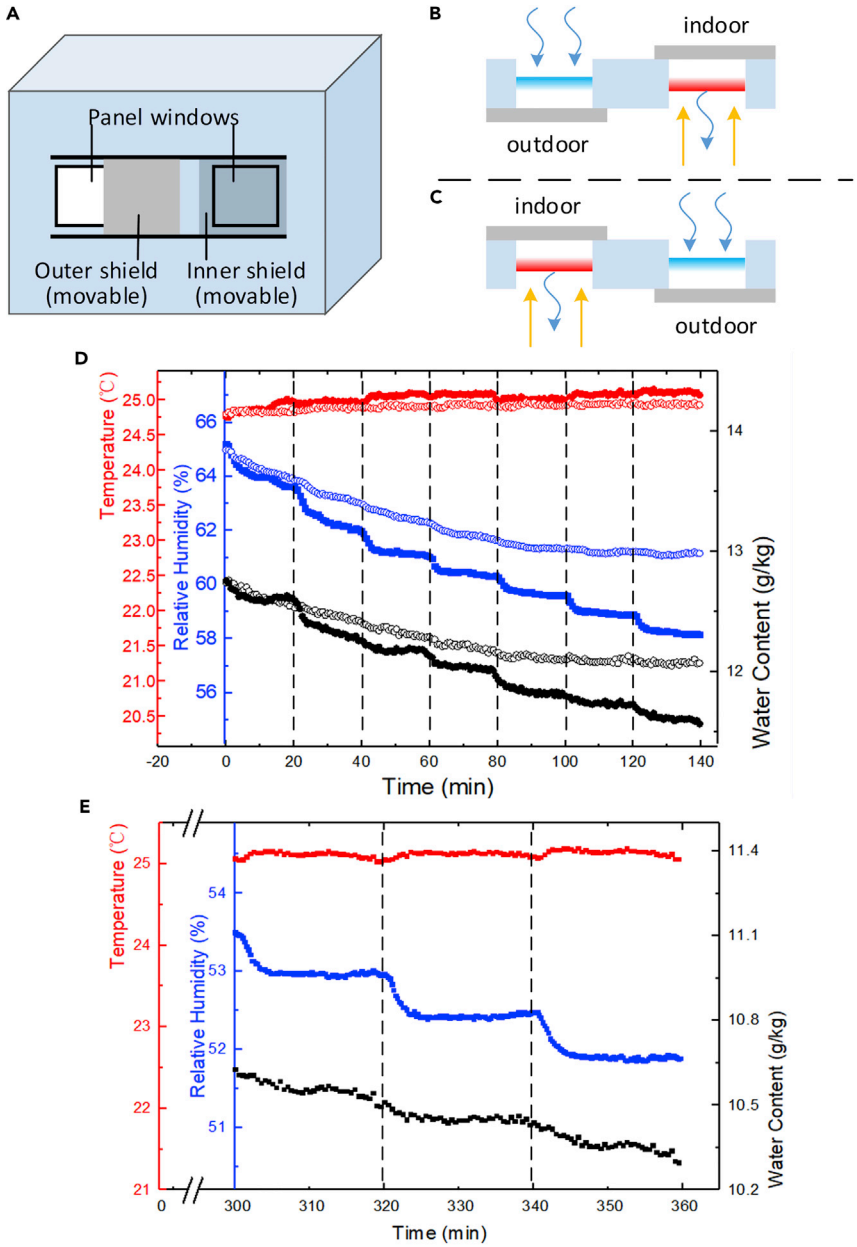

Figure 4. Illustration of Proof-of-Concept Prototype for Moisture-Permeable Panel Performance Evaluation

(A) The setup of scaled down model.

(B–D) (B) and (C) present the working process. The panel under sunlight illumination is losing water, whereas the one shielded from sunlight is adsorbing water vapor from indoor air. (D) System performance of different panels: panels with loose SG layer (open cycles) and panels with SG-MIL101(Cr) layer (closed cycles). The red, blue, and black symbols represent the temperature (°C), relative humidity (%), and water content of the air (g/kg), respectively. Vertical dashed lines indicate the switching time period (20 min).

(E) The system performance of SG-MIL101(Cr) panel close to medium RH level (around 50%). The red, blue, and black symbols represent the temperature (°C), relative humidity (%), and water content of the air (g/kg), respectively.

where H_{de} is the phase change enthalpy of removed water and Q_{input} is the total energy of the incident sunlight. For simplicity, we consider the humidity pump with 1 m^2 of panel and the working time is 1 h.

$$H_{de} = \Delta d * H_{water} = 33.8g * 2513Jg^{-1} = 8.5 * 10^4 J \quad \text{(Equation 8)}$$

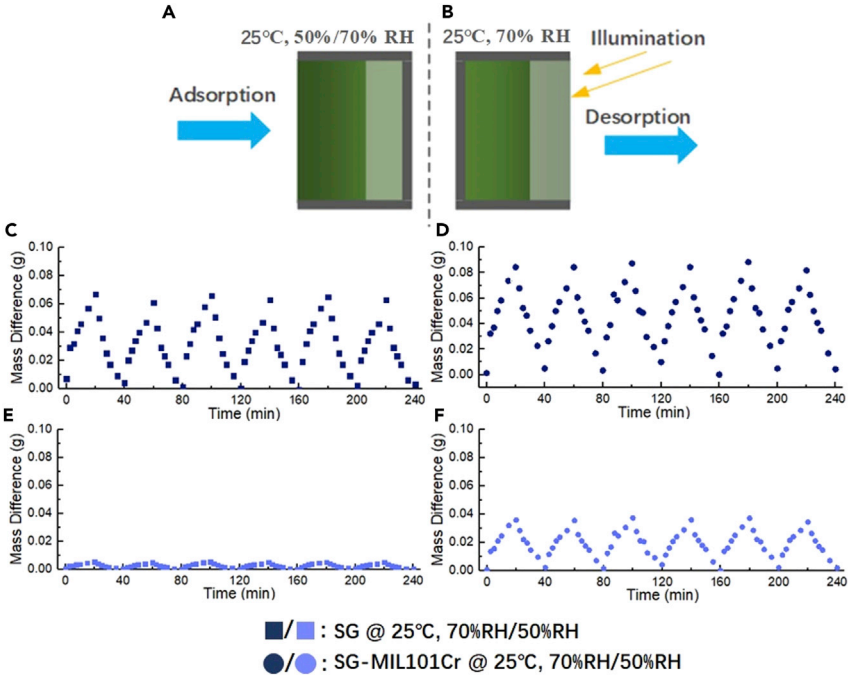

Figure 5. The Adsorption-Desorption Cycles

The experimental setup of adsorption (A) and desorption (B) processes are shown. Two different working conditions are chosen for adsorption process, whereas only one constant working condition is applied for desorption. The mass differences of the cycles of SG panel at (C) 25°C, 70% RH and (D) 25°C, 50% RH, SG-MIL101Cr panel at (D) 25°C, 70% RH and (E) 25°C, 50% RH are shown.

$$Q_{input} = I_0 * t = 10^3 Wm^{-2} * 3600s = 3.6 * 10^6 J \quad \text{(Equation 9)}$$

Therefore the energy efficiency η is 2.36%. It should be noted that higher efficiency can be expected with rational improvements, e.g., new water capture material with much higher water capacity or optimized structure that allows higher permeability. See Supplemental Information for details (Transparent Methods, Energy Efficiency).

The adsorption-desorption cycle test was carried out to better understand the difference between SG panel and SG-MIL101Cr panel. The adsorption processes were carried out at different conditions: 25°C, 70% RH and 25°C, 50% RH, whereas the desorption processes were taken under one constant working condition: 25°C, 70% RH (the desorption only takes place on the outside surface, where the environment condition is considered as constant). The mass difference of each cycle represents the water transportation ability of each sample under certain conditions. The adsorption and desorption were carried out alternatively using different setups (Figures 5A and 5B) with a period of 20 min. During this process, the mass change of each sample was measured and recorded. Both samples have the same dimension of 3 cm × 3 cm. Six stable cycles were chosen and shown in Figures 5C–5F. The squares stand for SG panels, whereas the cycles represent SG-MIL101Cr panels. Under 25°C, 70% RH, both SG (Figure 5C) and SG-MIL101Cr (Figure 5D) panels have satisfactory mass differences, 0.07 and 0.084 g, respectively, which is equal to the effective amount of water transported per cycle. The better performance of the composite panel may result from the larger water uptake ability of MIL101Cr. Under 25°C, 50% RH, however, the mass differences of both samples decreased a lot, especially for SG panel (Figure 5E). Roughly 0.005 g per cycle is observed. The mass difference of SG-MIL101Cr sample (Figure 5F), although decreases, still remains at a moderate value of 0.04 g. It is very clear that under such medium RH condition as well as the photothermal-driven condition on the outside surface, the SG panel loses most of the water capture ability because the difference of water uptake amount between the indoor and outdoor working conditions is too small to provide enough positive moisture potential as the mass transfer-driven force. On the other hand, MIL101Cr can still keep an adsorption-desorption cycle with obvious water uptake amount according to its isotherms. Therefore it is evident that the

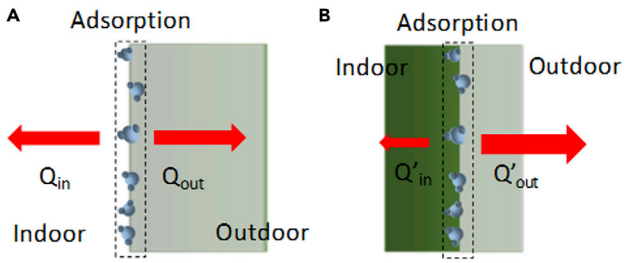

Figure 6. Schematic Diagram of Heat Transfer in Adsorption Process

(A and B) (A) Panel without a porous matrix layer inside. Most of the heat is transferred to indoor air via convection; (B) panel with a porous matrix layer. Most of the heat is transferred to outdoor space.

SG-MIL101Cr panel not only performs better in the high-RH region but also can successfully reduce the indoor RH down to medium RH level.

DISCUSSION

Estimation of Latent Sensible Heat Load Conversion

The introduction of this solar humidity pump may realize the independent control of temperature and humidity. Usually when certain amount of moisture is adsorbed by solid desiccant, the corresponding amount of latent heat is converted into sensible in the form of adsorption heat (Maclaine-Cross and Banks, 1972). If handled improperly, most of this heat may increase the overall indoor heat load and diminish the energy conservation introduced by this solar humidity pump. A detailed mathematical modeling is beyond the scope of this article, but a brief estimation is necessary and enough to demonstrate the idea of structure design. As the dynamic adsorption curve shows (Figure S2), the porous PF layer may influence the overall WVT ability of the panel. However, the PF has such an excellent thermal insulation property that it may greatly weaken the heat loss of the panel, and therefore the little influence on mass transfer can be neglected. If the desiccant layer is in direct contact with the indoor air (Figure 6A), the heat flux to indoor (Q_1) and outdoor (Q_2) can be expressed as:

$$Q_{in} = h \cdot A \cdot \Delta t \qquad \text{(Equation 10)}$$

$$Q_{out} = \frac{\lambda_{SG}}{\delta_{SG}} \cdot A \cdot \Delta t \qquad \text{(Equation 11)}$$

For simplicity, we consider a simple natural convection condition, where the h is around 10 W/m^{2}K. The thermal conductivity of the SG layer is around 0.1 W/mK and the sample thickness 1 cm, thus the value of λ_{SG}/δ_{SG} is also around 10 W/m^{2}K. So under such condition, the Q_{in} roughly equals Q_{out}. In comparison, by introducing the multilayer structure (Figure 6B), the water vapor should first go through the porous PF layer before it reaches the SG layer interface. Similarly, the adsorption heat transfer path Q'_{in} and Q'_{out} can be written as:

$$Q'_{in} = \frac{\lambda_{PF}}{\delta_{PF}} \cdot A \cdot \Delta t \qquad \text{(Equation 12)}$$

$$Q'_{out} = \frac{\lambda_{SG}}{\delta_{SG}} \cdot A \cdot \Delta t \qquad \text{(Equation 13)}$$

The thermal conductivity of pure PF layer is only around 0.03 W/mK, and in this research the thickness of PF matrix layer is identical to that of the SG layer. Therefore the value of λ_{PF}/δ_{PF} is around 3 W/m^{2}K. Under such condition, the value of Q'_{in} equals 30% of Q'_{out}. Furthermore, the thickness of the PF layer δ_{PF} can be much larger than it was in this research and consequently leads to a much smaller Q'_{in} value and Q'_{in}:Q'_{out} ratio.

Potential Applications

A bright future for a broad application of such moisture pump is expected. Potential application situations may include commercial and residential buildings, industrial plants, and electronic devices. Such moisture pump can be easily integrated with construction materials so that a moisture-permeable wall or window is expected. Thus the indoor latent heat load can be independently handled by this humidity pump in the daytime, resulting in a higher efficiency of the cooling unit, which could only deal with the sensible heat load. Consider a department with an area of 25 m^2 and one inhabitant inside. The required panel area is around 5.6 m^2 to fully cover the moisture load (see details in Transparent Methods, Real World

Application). Similar construction structures can be expected in industrial plants, but with much larger scale. The performance-price ratio of this humidity pump is the same as or even better than that of the solar photovoltaic-driven air-conditioning system (see details in Transparent Methods, Performance-Price Ratio). Another application situation is the humidity control inside some precise electronic devices. The moisture often appears as a disaster inside the precise electronic devices, which may disable the current circuit or even destroy the whole device. A common approach to remove the moisture inside the device can be achieved by drying with hot wind, but this requires the unsealing of the device, which may bring in other impurities or damage the mechanical parts during disassembly or assembly. By applying such microscale humidity pump, the moisture removal process is available without the need to disassemble the device, leaving no risk of further damage or impurity introduction. Under such circumstances, the heat source is no longer limited as sunlight, but could be any kind of surface heating technology.

Limitations of the Study

The sun illumination condition applied in the experiment is idealized. This research is a proposal of a concept and its validation rather than a systematic study of such humidity pump system. Therefore the sun illumination condition is simplified to better understand the working mechanism and the performance criteria. However, under real conditions, the solar radiation usually grazes the building facade rather than incident perpendicularly, thus solar radiation model should be then considered to better evaluate the working performance under real conditions. Such work should be carried out in a more systematic investigation of such humidity pump system, which includes the performance tests of some standard working conditions.

Besides, this humidity pump still suffers from a relatively low dehumidification rate compared with both vapor compression system and conventional solid desiccant cooling system. The relatively poor water vapor transfer ability is the dominant reason. The key to improve this issue very largely lies both on the material science, which may provide more appropriate candidate desiccants, and structure design, which could optimize the facility with aligned channels and good thermal insulation, if possible. The material fabrication and selection, as well as the structure optimization, would be a long-term work, which, when fulfilled, may largely improve the dehumidification rate of this humidity pump.

METHODS

All methods can be found in the accompanying Transparent Methods supplemental file.

SUPPLEMENTAL INFORMATION

Supplemental Information can be found online at https://doi.org/10.1016/j.isci.2019.05.013.

ACKNOWLEDGMENTS

This research was financially supported by the Foundation for Innovative Research Groups of the National Natural Science Foundation of China (Grant No. 51521004). We thank the members of ITEWA (Innovative Team for Energy Water and Air) of Shanghai Jiao Tong University (SJTU) for their discussion and suggestions given during the manuscript writing. We thank Ms. Lingji Hua from Institute of Refrigeration and Cryogenic, SJTU, for her support in model establishment. We thank Prof. Tao Deng and Yanming Liu from the School of Material Science and Engineering, SJTU, for their help in the photothermal experiments.

AUTHOR CONTRIBUTIONS

B.C. developed the concept, conducted the experiments, analyzed the data, and wrote the paper. Y.T. proposed several helpful suggestions on experiments and revised the manuscript. R.W. directed the overall research and revised the manuscript.

DECLARATION OF INTERESTS

The authors have no competing financial interests.

Received: March 15, 2019
Revised: April 18, 2019
Accepted: May 9, 2019
Published: May 31, 2019

REFERENCES

Allouhi, A., Kousksou, T., Jamil, A., Bruel, P., Mourad, Y., and Zeraouli, Y. (2015). Solar driven cooling systems: an updated review. Renew. Sustain. Energy Rev. *44*, 159–181.

Anand, S., Gupta, A., and Tyagi, S.K. (2015). Solar cooling systems for climate change mitigation: a review. Renew. Sustain. Energy Rev. *41*, 143–161.

Chu, S., and Majumdar, A. (2012). Opportunities and challenges for a sustainable energy future. Nature *488*, 294–303.

Costa, A., Keane, M.M., Torrens, J.I., and Corry, E. (2013). Building operation and energy performance: monitoring, analysis and optimisation toolkit. Appl. Energy *101*, 310–316.

Daou, K., Wang, R.Z., and Xia, Z.Z. (2006). Desiccant cooling air conditioning: a review. Renew. Sustain. Energy Rev. *10*, 55–77.

Deng, S., Wang, R.Z., and Dai, Y.J. (2014). How to evaluate performance of net zero energy building - a literature research. Energy *71*, 1–16.

Farese, P. (2012). How to build a low-energy future. Nature *488*, 275–277.

Ferey, G. (2005). A chromium terephthalate-based solid with unusually large pore volumes and surface area. Science *309*, 2040–2042.

Ge, T.S., Li, Y., Wang, R.Z., and Dai, Y.J. (2009). Experimental study on a two-stage rotary desiccant cooling system. Int. J. Refrig. *32*, 498–508.

Grossman, G. (2002). Solar-powered systems for cooling, dehumidification and air-conditioning. Solar Energy *72*, 53–62.

Hong, D.-Y., Hwang, Y.K., Serre, C., Ferey, G., and Chang, J.-S. (2009). Porous chromium terephthalate MIL-101 with coordinatively unsaturated sites: surface functionalization, encapsulation, sorption and catalysis. Adv. Funct. Mater. *19*, 1537–1552.

Kalmutzki, M.J., Diercks, C.S., and Yaghi, O.M. (2018). Metal-organic frameworks for water harvesting from air. Adv. Mater. *30*, e1704304.

Khutia, A., Rammelberg, H.U., Schmidt, T., Henninger, S., and Janiak, C. (2013). Water sorption cycle measurements on functionalized MIL-101Cr for heat transformation application. Chem. Mater. *25*, 790–798.

Kim, H., Yang, S., Rao, S.R., Narayanan, S., Kapustin, E.A., Furukawa, H., Umans, A.S., Yaghi, O.M., and Wang, E.N. (2017). Water harvesting from air with metal-organic frameworks powered by natural sunlight. Science *356*, 430–432.

La, D., Dai, Y.J., Li, Y., Wang, R.Z., and Ge, T.S. (2010). Technical development of rotary desiccant dehumidification and air conditioning: a review. Renew. Sustain. Energy Rev. *14*, 130–147.

Liu, Q., Ning, L., Zheng, S., Tao, M., Shi, Y., and He, Y. (2013). Adsorption of carbon dioxide by MIL-101(Cr): regeneration conditions and influence of flue gas contaminants. Sci. Rep. *3*, 2916.

Liu, Y., Chen, J., Guo, D., Cao, M., and Jiang, L. (2015a). Floatable, self-cleaning, and carbon-black-based superhydrophobic Gauze for the solar evaporation enhancement at the air-water interface. ACS Appl. Mater. Interfaces *7*, 13645–13652.

Liu, Y., Yu, S., Feng, R., Bernard, A., Liu, Y., Zhang, Y., Duan, H., Shang, W., Tao, P., Song, C., and Deng, T. (2015b). A bioinspired, reusable, paper-based system for high-performance large-scale evaporation. Adv. Mater. *27*, 2768–2774.

Maclaine-Cross, I.L., and Banks, P.J. (1972). Coupled heat and mass transfer in regenerators-prediction using an analogy with heat transfer. Int. J. Heat Mass Transf. *15*, 1225–1242.

Marszal, A.J., Heiselberg, P., Bourrelle, J.S., Musall, E., Voss, K., Sartori, I., and Napolitano, A. (2011). Zero Energy Building - a review of definitions and calculation methodologies. Energy Build. *43*, 971–979.

Mei, L., and Dai, Y.J. (2008). A technical review on use of liquid-desiccant dehumidification for air-conditioning application. Renew. Sustain. Energy Rev. *12*, 662–689.

Mekonnen, M.M., and Hoekstra, A.Y. (2016). Four billion people facing severe water scarcity. Sci. Adv. *2*, e1500323.

Ni, G., Li, G., Boriskina, S.V., Li, H., Yang, W., Zhang, T., and Chen, G. (2016). Steam generation under one sun enabled by a floating structure with thermal concentration. Nat. Energy *1*, https://www.nature.com/articles/nenergy2016126.

Nkwetta, D.N., and Sandercock, J. (2016). A state-of-the-art review of solar air-conditioning systems. Renew. Sustain. Energy Rev. *60*, 1351–1366.

Otanicar, T., Taylor, R.A., and Phelan, P.E. (2012). Prospects for solar cooling - an economic and environmental assessment. Solar Energy *86*, 1287–1299.

Panaras, G., Mathioulakis, E., and Belessiotis, V. (2011). Solid desiccant air-conditioning systems - design parameters. Energy *36*, 2399–2406.

Pesaran, A.A., and Mills, A.F. (1987a). Moisture transport in silica gel packed beds. I. Theoretical study. Int. J. Heat Mass Transf. *30*, 1037–1049.

Pesaran, A.A., and Mills, A.F. (1987b). Moisture transport in silica gel packed beds. II. Experimental study. Int. J. Heat Mass Transf. *30*, 1051–1060.

Rallapalli, P.B.S., Raj, M.C., Patil, D.V., Prasanth, K.P., Somani, R.S., and Bajaj, H.C. (2013). Activated carbon @ MIL-101(Cr): a potential metal-organic framework composite material for hydrogen storage. Int. J. Energy Res. *37*, 746–753.

Rotzetter, A.C.C., Schumacher, C.M., Bubenhofer, S.B., Grass, R.N., Gerber, L.C., Zeltner, M., and Stark, W.J. (2012). Thermoresponsive polymer induced sweating surfaces as an efficient way to passively cool buildings. Adv. Mater. *24*, 5352–5356.

Rupp, R.F., Vasquez, N.G., and Lamberts, R. (2015). A review of human thermal comfort in the built environment. Energy Build. *105*, 178–205.

Shukla, D.L., and Modi, K.V. (2017). A technical review on regeneration of liquid desiccant using solar energy. Renew. Sustain. Energy Rev. *78*, 517–529.

Tu, Y.D., Wang, R.Z., Ge, T.S., and Zheng, X. (2017). Comfortable, high-efficiency heat pump with desiccant-coated, water-sorbing heat exchangers. Sci. Rep. *7*, 40437.

Wan, J.W., Yang, K., Zhang, W.J., and Zhang, J.L. (2009). A new method of determination of indoor temperature and relative humidity with consideration of human thermal comfort. Build. Environ. *44*, 411–417.

Wang, Z., Liu, Y., Tao, P., Shen, Q., Yi, N., Zhang, F., Liu, Q., Song, C., Zhang, D., Shang, W., and Deng, T. (2014). Bio-inspired evaporation through plasmonic film of nanoparticles at the air-water interface. Small *10*, 3234–3239.

Yang, L., Yan, H., and Lam, J.C. (2014). Thermal comfort and building energy consumption implications - a review. Appl. Energy *115*, 164–173.

Zhang, T., and Liu, X.-H. (2016). Performance comparison of temperature and humidity independent control air-conditioning system with conventional system. BSER&T *37*, 479–488.

Zhang, T., Liu, X., and Jiang, Y. (2014). Development of temperature and humidity independent control (THIC) air-conditioning systems in China-A review. Renew. Sustain. Energy Rev. *29*, 793–803.

Zhao, H.-X., and Magoules, F. (2012). A review on the prediction of building energy consumption. Renew. Sustain. Energy Rev. *16*, 3586–3592.

Zhao, K., Liu, X.-H., Zhang, T., and Jiang, Y. (2011). Performance of temperature and humidity independent control air-conditioning system in an office building. Energy Build. *43*, 1895–1903.

Zheng, X., Ge, T.S., Jiang, Y., and Wang, R.Z. (2015a). Experimental study on silica gel-LiCl composite desiccants for desiccant coated heat exchanger. Int. J. Refrig. *51*, 24–32.

Zheng, X., Ge, T.S., and Wang, R.Z. (2014). Recent progress on desiccant materials for solid desiccant cooling systems. Energy *74*, 280–294.

Zheng, X., Wang, R.Z., Ge, T.S., and Hu, L.M. (2015b). Performance study of SAPO-34 and FAPO-34 desiccants for desiccant coated heat exchanger systems. Energy *93*, 88–94.

ISCI, Volume *15*

Supplemental Information

A Moisture-Penetrating Humidity Pump Directly Powered by One-Sun Illumination

Biye Cao, Yaodong Tu, and Ruzhu Wang

Figure S1

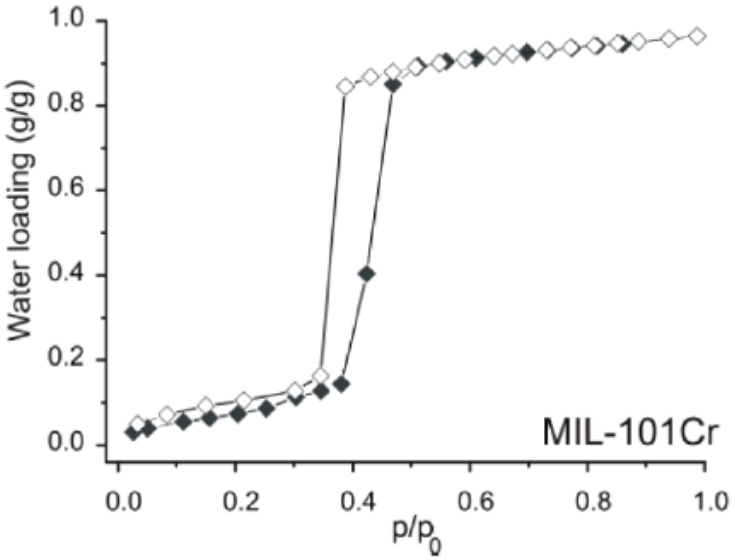

Figure S1. The water adsorption isotherm of pure MIL-101(Cr) measured by A. Khutia et. al.(Khutia et al., 2013) Closed and open marks represent the adsorption and desorption processes, respectively. Related to Figure 2.

Fig. S2.

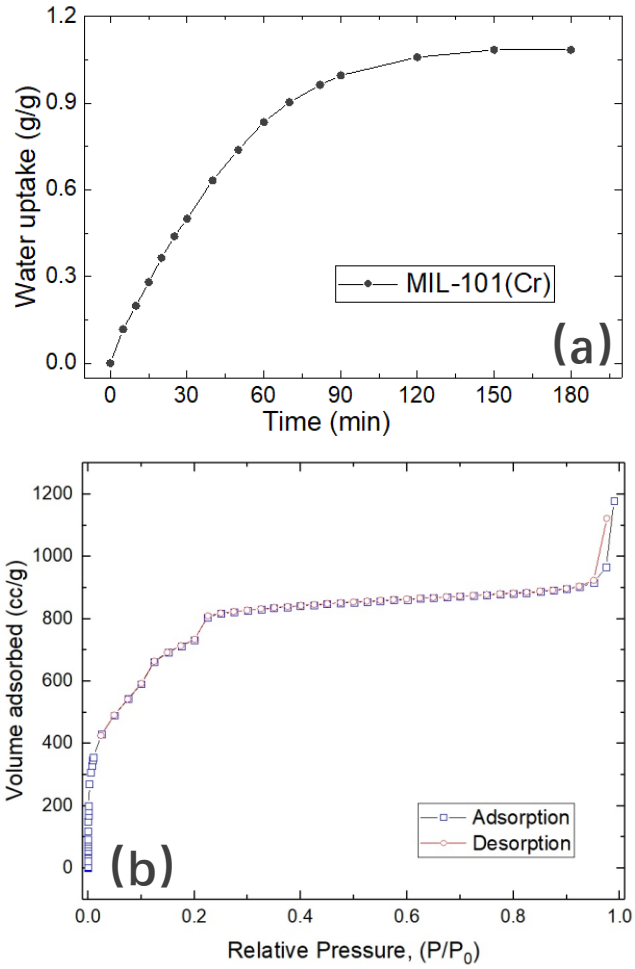

Figure S2. Dynamic water adsorption of MIL101(Cr) (a) and nitrogen adsorption test (b). The dynamic water adsorption as well as the nitrogen adsorption test of the MIL101(Cr) were carried out to evaluate the quality of the MOF we prepared. The dynamic adsorption (a) was carried out at 25℃, 70%RH and a final water uptake of 1.08g/g is obtained. From the nitrogen adsorption (b) result, the BET surface area can be calculated as 2906 m^2/g. Related to Figure 2.

Fig. S3.

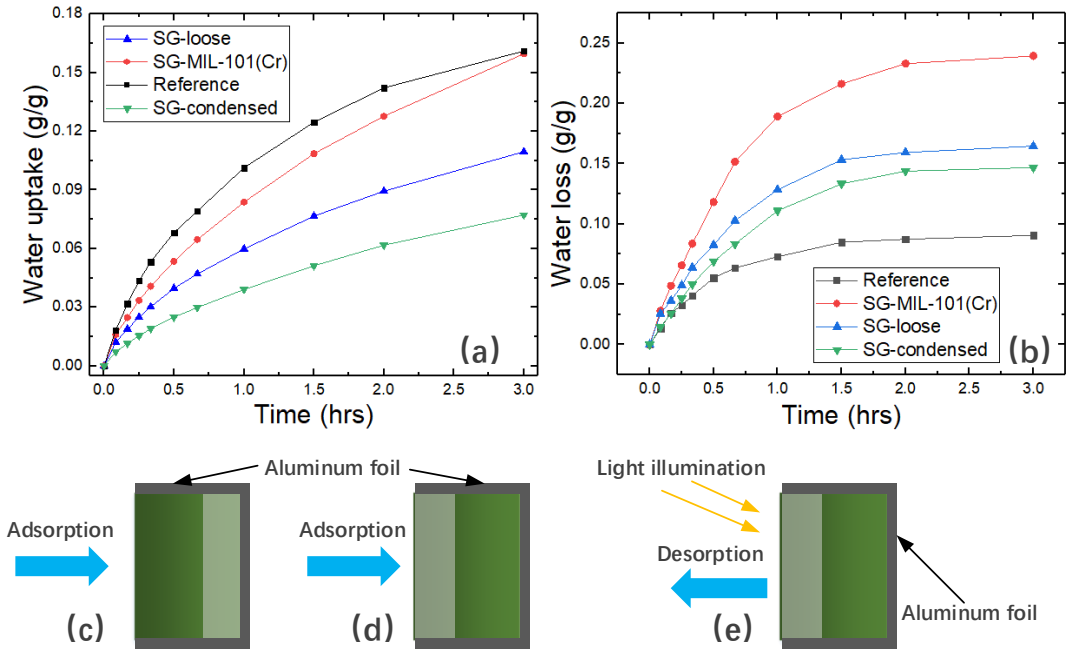

Figure S3. The dynamic adsorption(a) and desorption(b) curves. To completely meet the real working conditions, all the adsorption measurements were carried out with the process shown in (c) while (d) stands for the curve SG(reference). All the desorption measurements were taken using the setup (e). Related to Figure 2 and Table 1.

Fig. S4.

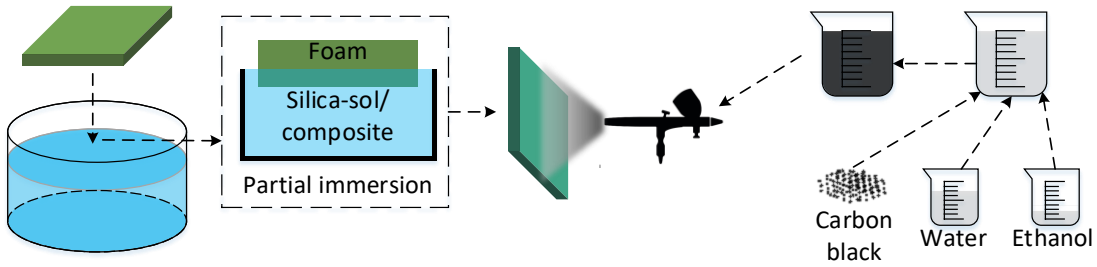

Figure S4. Fabrication steps of moisture permeable panel. The volume ratio of water and ethanol applied for CB suspension is 3:1. In the partial immersion, the liquid is either silica-sol or the composite of silica-sol and MIL101(Cr) suspension. Related to Figure 1.

Fig. S5.

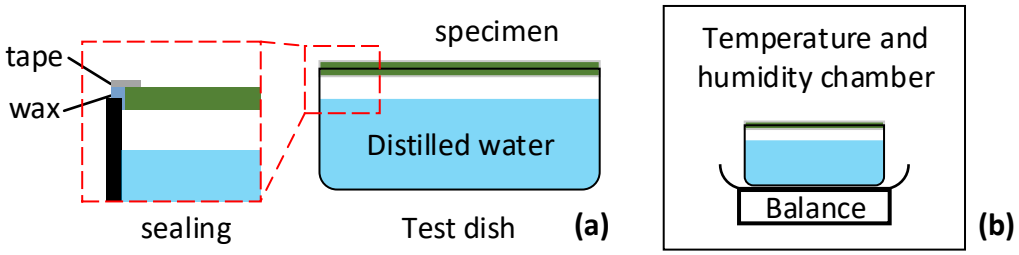

Figure S5. Apparatus of Water Vapor Transmission test. (a) specimen attachment and sealing details. Wax is used as sealant and tapes cover the wax as insurance. (b) the apparatus should be placed in a temperature and humidity chamber to control the surrounding environment. Related to Figure 2.

Fig. S6

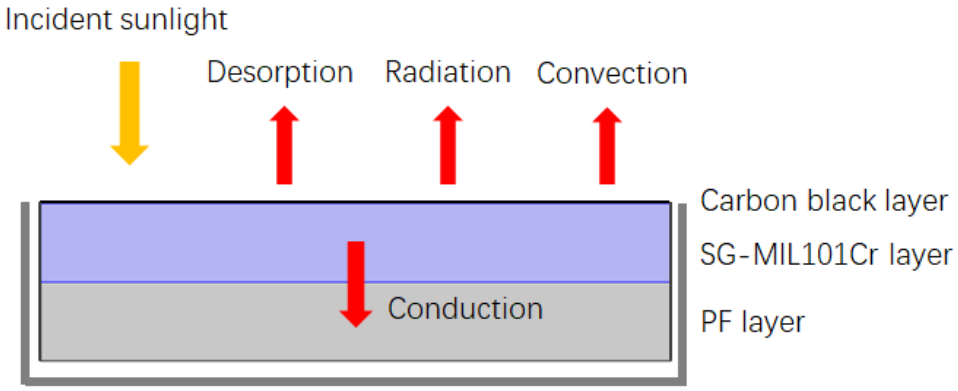

Figure S6. The heat transfer model during desorption stage. Related to Figure 3 and Figure 6.

Fig. S7

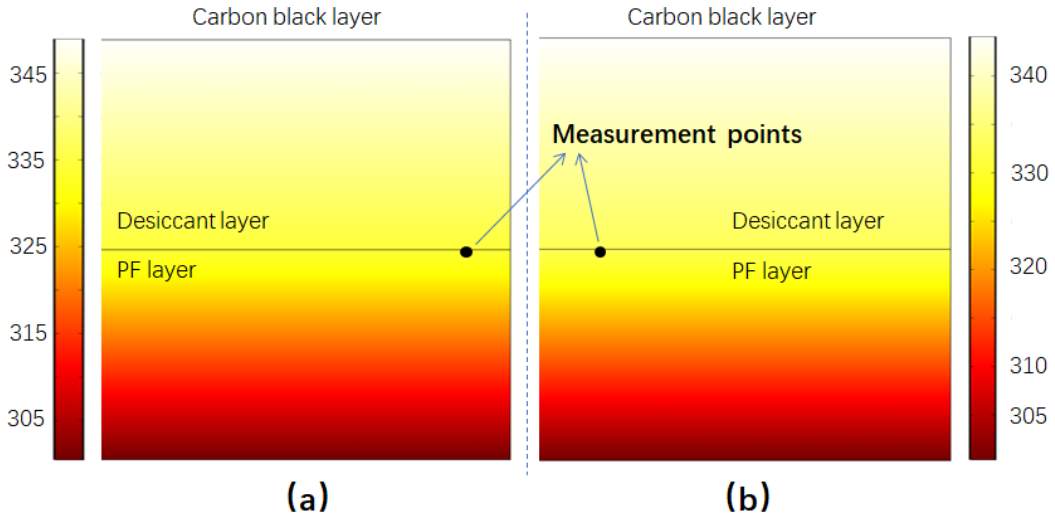

Figure S7. Simulation of temperature profile with dry (a) and wet (b) desiccant layers. Two measurement points are selected on the interface between the desiccant layer and the PF layer. Related to Figure 3 and Figure 6.

Table S1. Gluing amount of different kinds of moisture permeable panels. Related to Figure 2.

Panel description	SG-loose	SG-condensed	SG-MIL-101(Cr)
Gluing rate (g/cm^2)	0.165	0.338	0.177*

*The gluing amount of SG-MIL-101(Cr) comes from the total weight/total area. The SG-MIL-101(Cr) composite desiccant is pre-mixed with a fixed ratio.

Table S2. Detailed information of IR images. Related to Figure 3.

Panel number - Time	Average T (℃)	Std. Dev. (℃)	Max/Min T (℃)
a – 0 min	25.8	0.3	26.5/24.8
a – 5min	37.7	1.5	40.1/32.8
a – 30min	40.3	2.7	43.3/33.8
b – 0 min	25.3	0.1	25.7/24.8
b – 5 min	56.7	3.4	62.3/44.8
b – 30 min	58.5	2.7	62.6/49.2
c – 0 min	24.7	0.2	25.5/24.2
c– 5min	47.0	1.9	50.7/40.4
c – 30min	55.8	3.3	60.7/44.5
d –0 min	24.9	0.1	25.4/24.4
d – 5 min	58.4	2.8	62.6/49.6
d – 30 min	60.6	2.2	64.0/52.6

*The emissivity is 0.9 and the detect distance is 1 meter.

Table S3. Adsorption and desorption rates for all the samples. Related to Figure 2 and Figure 5.

Sample	SG-MIL-101(Cr)	SG loose	SG condensed	Reference
Adsorption(s^{-1})	$1.02x10^{-4}$	$8.50x10^{-5}$	$5.95x10^{-5}$	$2.02x10^{-4}$
Desorption(s^{-1})	$5.41x10^{-4}$	$2.42x10^{-4}$	$2.47x10^{-4}$	$6.45x10^{-5}$

Table S4, Materials and costs involved in panel fabrication. Related to Figure 4.

Material	Amount	Total price (in RMB/USD)
PF	$0.01m^3$	10/1.5
SG(30 wt% silica-sol)	1.65kg(5.5kg)	50/7.5
Carbon black powder	10g	20/3
Cr(NO3)3	533g	30/4.5
H2BDC	220g	35/5.2
Solvents and electricity	-	25/3.7
Summary	-	170/25.5

* $Cr(NO_3)_3$ and H_2BDC are the row chemicals for MIL101(Cr) fabrication.

Transparent Methods

MIL101(Cr) synthesis. The synthesis of MIL101(Cr) was following the reported method(Ferey, 2005). The chromium (III) nitrate $Cr(NO_3)_3{\cdot}9H_2O$ (purchased from X) and H_2BDC (1,4-benzenedicarboxylic acid) were involved in the synthesis of MIL-101(Cr). 4.0g of chromium (III) nitrate and 1.66g H_2BDC were dispersed in 50mL of deionized (DI) water in a 100-mL stainless steel pressure vessel. The mixture was stirred for 10 minutes and consequently treated by ultra-sonic for 15 minutes to avoid aggregations. The pressure vessel was placed in an oven under a programmed heating-cooling process. The temperature rose from RT to 220℃ with a rate of 0.2℃/min, and was kept at 220℃ for 8 hours. Then cooling process is controlled at 0.2℃/min drop. Deep green suspension was acquired through this procedure. The SG-MIL101(Cr) composite desiccant was achieved by a pre-mix of MIL101(Cr) suspension and silica-sol in a controlled ratio (mass ratio of 1:10, see mass ratio control of the SG-MIL101(Cr)) and the mixed suspension is stirred overnight to ensure a total dispersion. The suspension was involved in the further steps (to form composite suspension with silica-sol)but MOF powders were also prepared for characterization such as dynamic water adsorption and nitrogen sorption (Figure S2)

Moisture permeable panel fabrication. The fabrication of moisture permeable panel can be divided into three major steps, including matrix pre-cleaning, desiccant layer formation and photo-thermal layer coating. The matrix foam was cut into 10cm*10cm pieces of panel with 1.0cm thickness. All the foam panels were thoroughly washed and dried to remove impurities. The loose layer was achieved by partially immerse the panel into silica-sol for 5 seconds. Similarly, the composite layer was obtained by immerse the panel into mixed suspension acquired above for 5 seconds. The condensed layer was obtained by multi-time immersion (3 times in this research). Then all panels were put into an oven under 65℃ for 24 hours. After the completion of desiccant layer, the surface was covered with nano size carbon black powder by suspension spraying method. The ethanol-water liquid mixture (1:4 in volume proportion) was introduced to reduce the hydrophobicity of CB powders. This liquid mixture can contribute a lot to the complete and

average dispersion of carbon black powder in the suspension. The suspension was prepared in a concentration of 0.1g/20mL. 10 minutes of shock and 15 minutes of ultra-sonic treatment are carried out to ensure the total and average dispersion. This suspension was put into a spray gun and 20mL of suspension was sprayed onto each panel surface (10cm*10cm). The panel was then placed in an oven under 65℃ for 4 hours. A water cleansing of the surface was introduced to remove the loosely attached carbon black powders (see Figure S4).

Water Vapor Transmission test. In the test of the Water Vapor Transmission experiment, a test dish, usually a beaker or a glass garden, was filled with controlled amount of distilled water and the specimen was attached to the test dish. The specimen was tightly sealed to the mouth of the test dish by aluminum foil and tapes to prevent any possible leakage. The water surface was controlled 19mm±6mm to the lower surface of the specimen, and the humid air above the liquid surface can be regarded as 100% relative humidity. This apparatus was placed in a temperature and humidity chamber to insure a constant environment outside the dish. An analytical balance was introduced to record the mass loss due to the water vapor difference between the two sides of the specimen. Sketch can be seen in Figure S5.

The sorption rate test

The dynamic adsorption (Figure S3a) and desorption (Figure S3b) measurements were carried out in the temperature-humidity constant room. All the samples were fully dried at 70℃ in an oven before adsorption under 25℃, 70%RH condition and all of them reached equilibrium at 25℃, 70%RH before desorption at 35℃, 70%RH, with one-sun illumination. The curves only present the performances of the first 3 hours which is critical for the dehumidification process. In adsorption process, the sample with SG-MIL-101(Cr) (red dots) achieves the best water uptake quantity (except the reference sample) while the sample with SG loose layer (blue triangles) only has a modest amount, demonstrating that the introduction of MIL-101(Cr) can largely improve the water uptake rate. The reference sample (black squares) has the same desiccant layer structure as the sample with SG loose layer, but very different water adsorption ability is observed. This is associated with the influence of PF foam which is introduced for thermal insulation, as described previously. The porous structure of PF foam, although accessible for water vapor transmission, clearly alleviates the water vapor transport ability and thus influence the water capture performance. However, identical equilibrium water adsorption quantity (0.181g/g) is acquired for both samples, indicating that the introduction of PF foam only reduces the water adsorption rate due to the tackle of the porous skeletons but scarcely influence the overall water uptake amount. In desorption process, the sample with SG-MIL-101(Cr) (red dots) losses water very fast while the reference sample (black squares) losses only a little. The surface temperature is considered as the dominating reasons. As illustrated in Figure S3, the IR images were taken to visualize the temperature distribution of the panels under one-sun illumination. The reference sample (a) and the CB coated sample (b) were both illuminated under one-sun condition and a temperature difference of 24℃ between the two samples are observed. The average temperature of (a) is around 38.2℃ while that of (b) can reach as much as 62℃. The side-view (c) clearly shows the temperature distribution along the normal vector of the panel surface. Steep temperature drop is observed ascribed to the excellent thermal insulation property of PF foam. The SG loose sample (blue triangles) and SG-condensed sample (green triangles) can desorb water much faster than the reference sample but still far from the SG-MIL-101(Cr) sample. This again shows the advantage of MIL-101(Cr) when losing water.

The LDF (linear driving force) model is applied to quantify the sorption rate [12]:

$$\frac{dx}{dt} = k(x - x_t) \quad (1)$$

where k stands for the rate coefficient (in s^{-1}), x for the equilibrium water uptake quantity (in g/g) and x_t for the dynamic water uptake quantity (in g/g). By combining eq. (1), the following equation is obtained:

$$-\ln\left(1 - \frac{x_t}{x}\right) = kt \quad (2)$$

The adsorption rate and desorption rate for all the samples are listed in Table S3.

The mass ratio control of the SG-MIL101(Cr)

The original MIL101(Cr) suspension was condensed to 0.1g/mL and was mixed with silica-sol (30% mass ratio) in a volumetric ratio of 3:5. Under such condition, the mass ratio of MIL101(Cr) and SG is 1:10. However, the addition of extra MIL101(Cr) suspension dilutes the silica sol, which may lead to a less mass ratio of the SG. Thus, the mixed suspension should be condensed again to re-gain the original mass-volume ratio of silica-sol. According to the volumetric ratio applied in the previous step, the volume of the condensed mixed suspension should be 62.5% that of the original mixed suspension.

Model and simulation

The carbon black powders are coated on the panel surface, and can convert the incident sunlight into heat via photo-thermal effect. Thus we can consider this layer as a surface heat source. The desiccant layer and PF layer are lying consequently under the carbon black layer with the same thickness of 0.5 cm. The left and right sides are considered as thermal insulated. (See Figure S6)
The thermal conductivity of PF layer is 0.035 $W \cdot m^{-1} \cdot K^{-1}$. The dominating equations are shown as follows:

$$q_{in} = q_{de} + q_{rad} + q_{cov} + q_{cod} + C_p m \frac{dT}{dt}$$

$$q_{in} = I_{in} * \eta$$

I_{in} stands for the intensity of incident sunlight, η the photo-thermal conversion efficiency.

$$q_{de} = \dot{m} * H$$

$\dot{m}$ stands for the desorption rate under illumination, H the phase change enthalpy of water.

$$q_{rad} = \varepsilon\sigma(T^4 - T_{amb}^4)$$

ε is the emittance of the carbon black surface. T and T_{amb} are surface and ambient temperatures, respectively. T_{amb} is set as 25°C according to the working condition.

$$q_{cov} = h(T - T_{amb})$$

$$q_{cod} = \lambda \frac{dT}{dx}$$

As the reviewer mentioned, two different situations should be considered: the desiccant layer is wet or partly dried. The thermal conductivities of each layer under two different conditions are measured: 0.08 $W \cdot m^{-1} \cdot K^{-1}$ when the desiccant is fully dried and 0.1 $W \cdot m^{-1} \cdot K^{-1}$ when the desiccant is wet under working condition. Besides, the q_{de} term also differs between two conditions: the water is desorbing very quickly when the layer is wet but becomes very slowly when the desiccant is dried. Therefore, the q_{de} term in wet layer is much larger than that of the dried layer. With a rough estimation, the q_{de} is set as 80 Wm^{-2} under wet condition and 10 Wm^{-2} under dried condition. The simulation results are shown in Figure S7 (only a zoomed-in area is shown for clearness).
From the results we can see that the temperature profiles of both conditions are similar and only a little difference is observed. Temperature of measurement points (on the interface between two

layers) are 334.16K for dry layer (a) and 332.72K for wet layer (b). Furthermore, the dry desiccant layer even has a higher temperature than the wet desiccant layer despite its lower thermal conductivity. This is mainly resulted from a much lower desorption rate which may consume a lot of heat. Therefore, although the desiccant is dried during the heating process and the thermal conductivity is reduced, the desiccant layer can still maintain an even higher temperature for continuous desorption.

Dehumidification rate:

The adsorption on the desiccant surface is usually expressed by following equation:

$$\frac{\partial W}{\partial t} = \frac{k}{\rho_d t_d}(Y_a - Y_d)$$

and inside the desiccant layer:

$$\frac{\partial(\rho_d W)}{\partial t} = \frac{\partial}{\partial z}[D_s \frac{\partial(\rho_d W)}{\partial z}]$$

Where W is the water uptake of the desiccant in g/g desiccant. ρ_d and t_d are the density and thickness of the desiccant. Y_a and Y_d stand for the water content of the ambient environment and in the desiccant, respectively, in g/kg air. D_s is the surface diffusion coefficient of water molecules inside the desiccant and k is the air-to-desiccant mass transfer coefficient.

In these equations, the W is connected with Y_d via the isotherms of the desiccant, and in fact, the W is strongly correlated with Y_d:

$$\mathrm{W} = W_d(\mathrm{T}, Y_d)$$
$$Y_d = f(T, W)$$

With a given temperature T, we can then obtain the W-Y_d relationship from the isotherms under this given temperature and the equation can be solved to obtain the W, which is exactly the water uptake of the desiccant during adsorption or desorption stage. The mass difference between the two stages can be considered as the humidity reduction amount and the humidity reduction rate can be consequently calculated.

$$r_{de} = \frac{\Delta W}{t_{cycle}}$$

Therefore, we can conclude from the above modeling that several parameters may influence the system performance. The water capacity of the desiccant W is an important parameter since it directly determines the adsorption quantity during each cycle. A larger adsorption quantity may lead to a higher humidity reduction rate. The mass transfer coefficients k and D_s are also dominating the performance. Larger coefficients may lead to higher adsorption quantity in the same adsorption period. The thermal conductivities of both desiccant layer and substrate (the PF layer in this paper) may also influence the system performance. On one hand, larger thermal conductivity of desiccant can lead to a higher-in-average temperature distribution in the desiccant layer, which may be helpful to the desorption process; On the other hand, a smaller thermal conductivity of substrate can prevent further heat loss by conduction via substrate, keeping more heat in the desiccant layer during desorption process.

Energy efficiency.

The energy efficiency η is 2.36%. But it should be noted that higher efficiency can be expected with rational improvements, e.g. new water capture material with much higher water capacity. Early this year (2019), Fei Zhao et.al.(Fei Zhao, 2019) reported a “super moisture-absorbent gels” which may potentially fulfill our needs. The PPy-Cl clusters aggregated on the gel matrix can

capture the water vapor in the air. Then the condensed water is transferred to the matrix (poly-NIPAM) for storage. Under 60% RH in room temperature, up to 3.4g/g water can be taken. This value is almost twice larger than that of MIL101Cr (~1.2g), and more than 5 times larger than that of SG (0.6g/g). If this super gel is applied, we can rationally expect a much larger water capacity of the panel with almost identical dimension, and consequently lead to a much better dehumidification rate. But since the lack of some related data (e.g. the isotherm under working condition, the permeability, the adsorption and desorption kinetics), it is difficult to quantitatively estimate the accurate values of potential efficiency currently.

Besides, the structure of the panel and the humidity pump, although have been optimized with our best, still has a great potential of improvements. Better mass transfer ability (permeability) can obviously accelerate the moisture transferring process and reduce the cycle period. If 20% enhancement of permeability is assumed, the cycle period can be reduced to 83% of what it originally is. This may lead to a 20% increase in dehumidification rate and consequently 20% higher in efficiency.

As we know, a conventional desiccant wheel solar dehumidification system may have a thermal COP around 0.4-0.6, but solar heating system as well as desiccant wheel air ducts should be installed, which could be another costive investment. Besides, such systems usually require manual control and frequent maintenance, and also occupy large spaces. This moisture penetrating humidity pump directly powered by one sun illumination has a simple structure and low cost, and may create a new insight for solar powered dehumidification.

Real world application:

Consider a department with area of 25 m^2(6.25 m length * 4 m width * 2.8 m height) with 1 inhabitant inside, the moisture load inside the department should be calculated as follows:

$$M_w = 0.001\varphi_B ng$$

φ_B stands for the assembly coefficient, n the number of inhabitant indoor and g the moisture release from an adult. Under such condition, 0.2kg/h of moisture load is introduced in this department. By using the best dehumidification rate we achieved in our paper, roughly 5.6 m^2 of such panels are needed to fully cover the moisture load, which equals to an area of 2.8m * 2m. This was based on the humidity pump operation period when sunshine is available. If we consider the moisture storage capability of the adsorbent layer, e.g. a moisture reservoir, a higher moisture adsorption capacity could be achieved, thus the humidity pump panel area could be further reduced.

We should mention that this moisture penetration humidity pump is only a proof-of-concept prototype, thus the results are not that competitive compared with the conventional dehumidification technologies. Several potential improvements may obviously increase the performance, including better desiccants with higher water capacity and moderate desorption temperature, optimized panel/pump structure with better mass transfer ability and thermal insulation, etc..

Besides, this humidity pump could also serve as a major dehumidifier to remove only part of the moisture load indoor instead of the whole. Under such condition, the efficiency of traditional AC system could be largely improved.

The performance-price ratio:

Since such humidity pump can directly utilize the solar illumination, metrics such as COP is not suitable for this system.

The fabrication of such panel involves several row materials and chemicals. Here we take 1 m^2 of such panel for the following calculation (see Table S4):

Please be noted that such costs are based on laboratory level, which can be largely decreased once it is industrially handled.

We can define a parameter PPR that can well describe the cost-performance relationship:

$$\text{PPR} = \frac{\text{unit price}}{r_{de}} = \frac{price}{1\ g\ (moisture\ load)/h}$$

Where unit price is the cost of panel with a certain area (1 m^2) in RMB(USD)/m^2, r_{de} the dehumidification rate of the panel with a certain area (1 m^2) in $gh^{-1}m^{-2}$. By using the data in our paper as well as the above mentioned total cost, the PPR of our humidity pump(HP) is PPR(HP)=5.0 RMB/1(g/h) (or 0.75 USD/1(g/h)). This value indicates that by achieving the ability to handle 1g of moisture load in 1 hour, the cost will be 5.0 RMB or 0.75 USD.

For comparison, a PV driven dehumidification system, which also utilize sunlight illumination as the energy source, is considered: The PV system receives sunlight and convert them into electricity. The generated electricity is then used for driving an AC system to remove the indoor moisture load. Typically, the COP of common AC system is around 3.0 which means by consuming 1J of electricity, 3J of heat load can be handled. Usually, 40% of the heat load is resulted from latent load or moisture load. Thus we can consider that by consuming 1J of electricity, 1.2J(=3J*40%) of moisture load is removed. The cost of solar PV module is usually around 8 RMB/1Wp. Using these parameters, we can obtain the PPR(PV) for a typical solar PV system:

$$1\text{g moisture load/h} = 2513\text{J moisture load/h} = 2094\text{J electricity/h}$$

$$\text{PPR(PV)} = \frac{8RMB}{1Wp} = \frac{8RMB}{3600J\ electricity/h} = \frac{8RMB}{1.71g\ moisture\ load/h} = 4.7RMB/1(g/h)$$

This shows that the solar PV system may cost 4.7RMB or 0.7 USD to achieve the ability to handle 1g moisture load in 1 hour. This cost is only slightly lower than that of our humidity pump system. However, this value only includes the solar PV system that generate electricity, the necessary pipes and air-conditioner are still not considered. It is hard to use the PPR parameter to value the pipes and air-conditioning facilities, but it is reasonable to estimate that the cost of solar PV-AC (PPR(PV-AC)) should be equal to or even higher than that of PPR(HP). Furthermore, it is still worthy to mention that the solar PV systems have been intensively studied for more than 30 years and increasing performance as well as the decreasing costs have been achieved. As above mentioned, this humidity pump is a new concept with very little optimization and improvements, and the costs are valued based on laboratory level rather than industrial level. We are confident, and also rational, to believe that our humidity pump may have a rising performance and falling cost with more detailed researches in the future.

References:

FEI ZHAO, G. Y. 2019. Super moisture absorbent geols for all weather atmospheric water harvesting. *Advanced Materials*.

FEREY, G. 2005. A chromium terephthalate-based solid with unusually large pore volumes and surface area (vol 309, pg 2040, 2005). *Science,* 310**,** 1119-1119.

KHUTIA, A., RAMMELBERG, H. U., SCHMIDT, T., HENNINGER, S. & JANIAK, C. 2013. Water Sorption Cycle Measurements on Functionalized MIL-101Cr for Heat Transformation Application. *Chemistry of Materials,* 25**,** 790-798.